Polar and Centrosymmetric Phases in Solid Solutions $Ca_{3-x}Sr_x(PO_4)_2$ ($0 \leqslant x \leqslant 16/7$)

A. A. Belik,[†,#] F. Izumi,[†] S. Yu. Stefanovich,[‡] A. P. Malakho,[§] B. I. Lazoryak,*[,‡] I. A. Leonidov,[∥] O. N. Leonidova,[∥] and S. A. Davydov[⊥]

Advanced Materials Laboratory, National Institute for Materials Science, 1-1 Namiki, Tsukuba, Ibaraki 305-0044, Japan, Departments of Chemistry and Materials Science, Moscow State University, Leninsky Gory, Moscow 119899, Russia, Institute of Solid State Chemistry, Pervomayskaia 91, Yekaterinburg 620219, Russia, and Institute of Metal Physics, Kovalevskaya 18, Yekaterinburg 620219, Russia

Received March 6, 2002

Solid solutions $Ca_{3-x}Sr_x(PO_4)_2$ ($0 \leq x \leq 16/7$) were studied by X-ray powder diffraction, infrared spectroscopy, differential scanning calorimetry, electrical-conductivity measurements, and second-harmonic generation. Phosphates with $0 \leq x \leq 12/7$ (β-phase) crystallize in space group $R3c$, $Z = 21$, $a \approx 10$ Å, and $c \approx 38$ Å. Sr-rich phosphates with $13/7 \leq x \leq 16/7$ (β'-phase) have a somewhat different crystal structure: space group $R\bar{3}m$, $Z = 10.5$, $a \approx 10$ Å, and $c \approx 19$ Å. The solid solutions with $0 \leq x \leq 12/7$ showed a reversible high-temperature phase transition $\beta \rightleftarrows \beta'$, where the β and β' phases have noncentrosymmetric and centosymmetric structures, respectively. The temperature of the phase transition decreased with increasing Sr content. In $Ca_3(PO_4)_2$, a new phase transition, $\beta \rightleftarrows \beta'$, was observed at 920 °C in the electrical-conductivity measurements. The structure parameters of polar β-$Ca_2Sr(PO_4)_2$ ($x = 1$) and centrosymmetric β'-$Ca_{5/7}Sr_{16/7}(PO_4)_2$ ($x = 16/7$) at room temperature were refined by Rietveld refinements of the X-ray diffraction data: space group $R3c$, $Z = 21$, $a = 10.5612(2)$ Å, and $c = 38.0588(5)$ Å for β-$Ca_2Sr(PO_4)_2$ and space group $R\bar{3}m$, $Z = 10.5$, $a = 10.7015(2)$ Å, and $c = 19.5787(2)$ Å for β'-$Ca_{5/7}Sr_{16/7}(PO_4)_2$. β-$Ca_2Sr(PO_4)_2$ is isotypic with β-$Ca_3(PO_4)_2$. In β-$Ca_2Sr(PO_4)_2$, the M4 site is 50% occupied by Sr^{2+} ions, and the M6 site is vacant. In both structures, Ca^{2+} and Sr^{2+} ions enter the M1−M3 sites whereas Ca^{2+} ions selectively occupy the M5 site. β'-$Ca_{5/7}Sr_{16/7}(PO_4)_2$ contains some disordered atoms: (1) cations at the M3 site are statistically distributed among several positions near the center of symmetry, (2) $P1O_4$ tetrahedra are orientationally disordered, and (3) the M4 site (M6 site in β-$Ca_2Sr(PO_4)_2$) is occupied by $0.165Sr^{2+} + 0.085Ca^{2+} + 0.75\square$. The mechanism of the $\beta \rightleftarrows \beta'$ phase transition in $Ca_{3-x}Sr_x(PO_4)_2$ ($0 \leq x \leq 12/7$) is discussed on the basis of the crystal data.

Introduction

Whitlockite[1] or β-$Ca_3(PO_4)_2$-like compounds,[2] for example, $Ca_9R(VO_4)_7$ (R = rare-earth metals and Bi),[3] have been extensively studied in expectation of their applications as nonlinear optical (NLO) materials.[4−8] In $Ca_9Bi(VO_4)_7$, its NLO signal is about 3 times as large as that of KH_2PO_4.[7] Tricalcium bis(phosphate), $Ca_3(PO_4)_2$, pure and doped with foreign cations has also been investigated as likely candidates for biomaterials,[9−12] luminescent materials,[13] and catalysts.[14]

Sarver et al.[15] constructed the phase diagram of a $Ca_3(PO_4)_2$−$Sr_3(PO_4)_2$ system at high temperatures. They found a new modification of tristrontium bis(phosphate), β-$Sr_3(PO_4)_2$, which was stable above 1305 °C and supposed to be isotypic with β-$Ca_3(PO_4)_2$[2] and whitlockite,

* To whom correspondence should be addressed. Tel.: 7-095-939-21-38. Fax: 7-095-938-24-57. E-mail: lazoryak@tech.chem.msu.ru.
[†] National Institute for Materials Science.
[‡] Department of Chemistry, Moscow State University.
[§] Department of Materials Science, Moscow State University.
[∥] Institute of Solid State Chemistry.
[⊥] Institute of Metal Physics.
[#] Postdoctoral fellow from Department of Chemistry, Moscow State University, Leninsky Gory, Moscow 119899, Russia.

(1) Calvo, C.; Gopal, R. *Am. Mineral.* **1975**, *60*, 120.
(2) Dickens, B.; Schroeder, L. W.; Brown, W. E. *J. Solid State Chem.* **1974**, *10*, 232.
(3) Lazoryak, B. I.; Dmitrienko, L. O.; Grechkin, S. V. *Russ. J. Inorg. Chem.* **1990**, *35*, 617.
(4) Kim, H. K.; Kim, M. S.; Park, S. M.; Sleight, A. W. *J. Cryst. Growth* **2000**, *219*, 61.
(5) Evans, J. S. O.; Huang, J.; Sleight, A. W. *J. Solid State Chem.* **2001**, *157*, 255.
(6) Lazoryak, B. I.; Belik, A. A.; Stefanovich, S. Yu.; Morozov, V. A.; Malakho, A. P.; Shelmenkova, O. V.; Leonidov, I. A.; Leonidova, O. N. *Dokl. Akad. Nauk* **2002**, *384*, 1.
(7) Sleight, A. W.; Huang, J. U.S. Patent 5202891, 1993.
(8) Belik, A. A.; Stefanovich, S. Yu.; Lazoryak, B. I. *Mater. Res. Bull.* **2001**, *36*, 1873.
(9) Rangavittal, N.; Landa-Canovas, A. R.; Gonzalez-Calbet, J. M.; Vallet-Regi, M. *J. Biomed. Mater. Res.* **2000**, *51*, 660.
(10) Langstaff, S.; Sayer, M.; Smith, T. J. N.; Pugh, S. M. *Biomaterials* **2001**, *22*, 135.
(11) Engin, N. O.; Tas, A. C. *J. Am. Ceram. Soc.* **2000**, *83*, 1581.
(12) Bigi, A.; Foresti, E.; Gandolfi, M.; Gazzano, M.; Roveri, N. *J. Inorg. Biochem.* **1997**, *66*, 259.
(13) Donker, H.; Smit, W. M. A.; Blasse, G. *J. Electrochem. Soc.* **1989**, *136*, 3130.
(14) Legrouri, A.; Lenzi, J.; Lenzi, M. *React. Kinet. Catal. Lett.* **1998**, *65*, 227.
(15) Sarver, J. F.; Hoffman, M. V.; Hummel, F. A. *J. Electrochem. Soc.* **1961**, *108*, 1103.

10.1021/cm020243l CCC: $22.00
Published on Web 06/08/2002

$Ca_{18.19}Mg_{1.17}Fe_{0.83}H_{1.62}(PO_4)_{14}$.[1] This high-temperature modification could not be quenched to room temperature (RT).[15] Nevertheless, β-$Sr_3(PO_4)_2$ proved to be stabilized at RT by doping various amounts of Mg^{2+}, Al^{3+}, Ca^{2+}, Zn^{2+}, or Cd^{2+} ions.[15−18] Solid solutions $Sr_{3-x}M_x(PO_4)_2$ with the β-$Sr_3(PO_4)_2$ structure have hitherto been prepared for M = Ca ($0.6 \le x \le 3$), M = Mg ($0.27 \le x \le 1.08$), M = Zn ($0.27 \le x \le 0.81$),[15] and M = Cd ($0.36 \le x \le 0.63$).[17] $Ca_{3-x}Sr_x(PO_4)_2$ was also studied by different authors.[12,19] Britvin et al.[20] described a mineral strontiowhitlockite, $Sr_9Mg(PO_3OH)(PO_4)_6$, which is an Sr derivative of synthetic whitlockite, $Ca_{18}Mg_2H_2(PO_4)_{14}$.[21] Sr-whitlockites containing Mg^{2+}, Mn^{2+}, Fe^{2+}, Co^{2+}, Ni^{2+}, Cu^{2+}, Zn^{2+}, or Cd^{2+} ions were synthesized by wet chemical processes[22] and a solid-state method.[23−25]

β-$Ca_3(PO_4)_2$ is stable at RT.[26,27] α-$Ca_3(PO_4)_2$,[28] stable between 1135 and 1430 °C, is quenchable to RT[27] whereas α'-$Ca_3(PO_4)_2$, stable above 1430 °C, is not quenchable. A new modification of tricalcium bis(phosphate), α''-$Ca_3(PO_4)_2$, was prepared from α-$Ca_3(PO_4)_2$ above 212 °C.[29] The temperature of the $\beta \rightleftarrows \alpha$ phase transition in $Ca_3(PO_4)_2$ strongly depended on the kind and amount of dopant. Doping small cations (Mg^{2+}, Zn^{2+}, Al^{3+}, and Fe^{3+}) or Sr^{2+} raised the temperature of the $\beta \rightleftarrows \alpha$ phase transition[15,30−33] while addition of Ca_2SiO_4, Ba^{2+}, or Cd^{2+} lowered the transition temperature. Experimental evidence for low-temperature phase transitions in $Ca_{3-x}M_x(PO_4)_2$ (M = Cu and Sn) was presented in the literature.[34−36]

In this work, we have studied solid solutions $Ca_{3-x}Sr_x(PO_4)_2$ ($0 \le x \le 17/7$) by X-ray powder diffraction (XRD), infrared (IR) spectroscopy, differential scanning calorimetry (DSC), electrical-conductivity measurements, and second-harmonic generation (SHG). We have found a new "polar-to-centrosymmetric" phase transition in these solid solutions. We have also determined the crystal structures of polar $Ca_{3-x}Sr_x(PO_4)_2$ ($x = 1$) and centrosymmetric $Ca_{3-x}Sr_x(PO_4)_2$ ($x = 16/7$) to clarify the mechanism of the phase transition. Our close investigation of the polar and centrosymmetric solid solutions will contribute to an understanding of the NLO properties of whitlockite-like materials.

Table 1. Conditions of the XRD Experiments and Parts of Refinement Results for β-$Ca_2Sr(PO_4)_2$ and β'-$Ca_{5/7}Sr_{16/7}(PO_4)_2$

	β-$Ca_2Sr(PO_4)_2$	β'-$Ca_{5/7}Sr_{16/7}(PO_4)_2$
space group	$R3c$ (No. 161)	$R\bar{3}m$ (No. 166)
Z	21	10.5
2θ range (°)	10−130	10−130
step width (°)	0.02	0.02
I_{max} (counts)	51549	83105
lattice parameters:		
a (Å)	10.5612(2)	10.7015(2)
c (Å)	38.0588(5)	19.5787(2)
V (Å^3)	3676.32(9)	1941.79(5)
no. of Bragg reflections	711	439
variables		
structure/lattice	65/2	31/2
background/profile	12/10	10/10
scale/peak shifts	1/2	1/2
PPP[a]	10	53
R_{wp}; R_p	5.96%; 4.37%	5.16%; 3.91%
R_B; R_F	1.75%; 0.88%	4.02%; 1.63%
S[b]	2.24	2.05

[a] Refined primary profile parameters.[38,39] [b] $S = R_{wp}/R_e$.

Experimental Section

Synthesis. Samples in the system $Ca_{3-x}Sr_x(PO_4)_2$ with $x = m/7$, where m is an integer from 0 to 17, were synthesized at 1000 °C for 120 h by the solid-state method from mixtures of $Ca_2P_2O_7$, $CaCO_3$, and $Sr_3(PO_4)_2$. The specimens were heated in alumina crucibles, ground every 30 h, and finally quenched in air.

XRD Experiments and Structure Refinements. XRD data of the samples were measured at RT on a SIEMENS D500 Bragg−Brentano-type powder diffractometer equipped with an incident-beam quartz monochromator to obtain Cu $K\alpha_1$ radiation ($\lambda = 1.5406$ Å) and a BRAUN position-sensitive detector and operated at 30 kV and 30 mA. Si was used as an external standard. For phase identification, XRD data were collected in a 2θ range from 10° to 60° with a step interval of 0.02°. The XRD data were analyzed by the Rietveld method[37] with RIETAN-2000[38,39] to refine lattice parameters. For structure refinements of $Ca_{3-x}Sr_x(PO_4)_2$ with $x = 1$ and 16/7, XRD data were collected on the above diffractometer with the experimental conditions given in Table 1. In what follows, the samples of $Ca_{3-x}Sr_x(PO_4)_2$ with $x = 1$ and 16/7 will be expressed as $Ca_2Sr(PO_4)_2$ and $Ca_{5/7}Sr_{16/7}(PO_4)_2$, respectively.

Structure parameters of the two samples were refined by the Rietveld method with RIETAN-2000 using atomic scattering factors for Sr^{2+}, Ca^{2+}, P, and O^-.[40] The split pseudo-Voigt function of Toraya[41] was fit to each reflection profile, and a ninth- or eleventh-order Legendre polynomial to the background. Partial profile relaxation[38,39] was applied to 012, 110, 015, 122, 205, 220, 404, 045, 324, 02$\bar{1}$0, and 22$\bar{1}$5 reflections for $Ca_{5/7}Sr_{16/7}(PO_4)_2$ and to 02$\bar{1}$0 and $\bar{2}$20 reflections for $Ca_2Sr(PO_4)_2$ to improve fits in these reflections in the last

(16) Koelmans, H.; Cox, A. P. M. *J. Electrochem. Soc.* **1957**, *104*, 442.
(17) Looney, J. R.; Brown, J. J. *J. Electrochem. Soc.* **1971**, *118*, 470.
(18) Levin, E. M.; Robbins, C. R.; McMurdie, H. F. *Phase Diagrams for Ceramists*; Reser, M. K., Ed.; The American Ceramic Society, Inc.: Columbus, OH, 1964; Figure 756.
(19) Nord, A. G. *Neues Jahrb. Mineral., Monatsh.* **1983**, *11*, 489.
(20) Britvin, S. N.; Pakhomovskii, Ya. N.; Bogdanova, A. N.; Skiba, V. I. *Can. Mineral.* **1991**, *29*, 87.
(21) Gopal, R.; Calvo, C.; Ito, J.; Sabine, W. K. *Can. J. Chem.* **1974**, *52*, 1155.
(22) Hashimoto, K.; Moriichi, N.; Toda, Y.; Saito, T.; Kanazawa, T.; Udagawa, S. *J. Soc. Inorg. Mater. Jpn.* (in Japanese) **1999**, *6*, 198.
(23) Belik, A. A.; Izumi, F.; Ikeda, T.; Lazoryak, B. I.; Morozov, V. A.; Malakho, A. P.; Stefanovich, S. Yu.; Grebenev, V. V.; Shelmenkova, O. V.; Kamiyama, T.; Oikawa, K.; Leonidov, I. A.; Leonidova, O. N.; Davydov, S. A. *Phosphorus, Sulfur, Silicon Relat. Elem.* **2002**, in press. Phosphorus *Chemistry*, July 29−August 3, Sendai, 2001; p 132.
(24) Belik, A. A.; Lazoryak, B. I.; Pokholok, K. V.; Terekhina, T. P.; Leonidov, I. A.; Mitberg, E. B.; Karelina, V. V.; Kellerman, D. G. *J. Solid State Chem.* **2001**, *162*, 113.
(25) Belik, A. A.; Malakho, A. P.; Lazoryak, B. I.; Khasanov, S. S. *J. Solid State Chem.* **2002**, *163*, 121.
(26) Fix, W.; Heymann, H.; Heinke, R. *J. Am. Ceram. Soc.* **1969**, *52*, 346.
(27) Monma, H.; Goto, M. *J. Ceram. Soc. Jpn.* **1983**, *91*, 473.
(28) Mathew, M.; Schroeder, L. W.; Dickens, B.; Brown, W. E. *Acta Crystallogr.* **1977**, *B33*, 1325.
(29) Ruan, L. J.; Wang, X. R.; Li, L. T. *Mater. Res. Bull.* **1996**, *31*, 1207.
(30) Ando, J. *Bull. Chem. Soc. Jpn.* **1958**, *31*, 196.
(31) Ando, J. *Bull. Chem. Soc. Jpn.* **1958**, *31*, 201.
(32) Kreidler, E. R.; Hummel, F. A. *Inorg. Chem.* **1967**, *6*, 524.
(33) Jakeman, R. J. B.; Cheetham, A. K.; Clayden, N. J.; Dobson, C. M. *J. Solid State Chem.* **1989**, *79*, 23.
(34) Mackay, A. L.; Sinha, D. P. *J. Phys. Chem. Solids* **1967**, *28*, 1337.
(35) Koelmans, H.; Engelsman, J. J.; Admiraal, P. S. *J. Phys. Chem. Solids* **1959**, *11*, 172.
(36) Romdhane, S. S.; Bonel, G.; Bacquet, G. *Mater. Res. Bull.* **1983**, *18*, 559.
(37) Rietveld, H. M. *J. Appl. Crystallogr.* **1969**, *2*, 65.
(38) Izumi, F.; Ikeda, T. *Mater. Sci. Forum* **2000**, *321−324*, 198.
(39) Izumi, F. *Rigaku J.* **2000**, *17*, 34.
(40) *International Tables for Crystallography*; Kluwer: Dordrecht, 1999; Vol. C, pp 572−574.
(41) Toraya, H. *J. Appl. Crystallogr.* **1990**, *23*, 485.

stage of the structure refinements. No preferred orientation was observed in the XRD patterns of the two samples.

SHG Experiments. SHG responses of powder samples were measured in a reflection scheme. A Q-switch pulsed Nd:YAG laser operated at $\lambda_\omega = 1064$ nm was used as a radiation source with a repetition rate of 4 impulses/s and a duration of impulses of about 12 ns. The laser beam was split into two beams to excite the radiation at a halved wavelength, $\lambda_{2\omega}$, of 532 nm simultaneously in samples to be measured and a reference sample: polycrystalline α-SiO_2. The incident-beam peak power was about 0.1 MW on a spot 3 mm in diameter on the surface of the sample. SHG signals were measured between 20 and 800 °C.

IR Spectroscopy, DSC, and Electrical-Conductivity Measurements. IR spectra were recorded on a Nicolet Magna-750 Fourier spectrometer in a wavenumber range of 4000−400 cm^{-1} using the KBr pellet technique. Specific heat capacities, c_p, were measured in air with a Setaram DSC-111 difference-scanning calorimeter between 20 and 815 °C at a heating rate of 5 °C/min. To measure the electrical conductivities, we used samples in the form of pellets 4−5 mm in length and 5−6 mm in diameter. They were pelletized by pressing at 1 kbar and sintering at 1050 °C for 10 h (cooling rate: 4 °C/min). The densities of the resultant pellets rose to 90% of theoretical densities. Pt electrodes were put on flat surfaces of the pellets. All the conductivities were measured by the impedance spectroscopy method in a frequency range of $1-10^6$ Hz with a Solatron 1260 frequency response analyzer.

Results

Characterization of the Solid Solutions. XRD showed that the samples of $Ca_{3-x}Sr_x(PO_4)_2$ with $0 \le x \le 16/7$ were monophasic. The sample with $x = 17/7$ consisted of two phases: a whitlockite-like phase and α-$Sr_3(PO_4)_2$.[42] The mass fraction of α-$Sr_3(PO_4)_2$ in this sample was calculated at 12.4% from refined scale factors. Then, the chemical composition of the whitlockite-like phase is represented as $Ca_{0.69}Sr_{2.31}(PO_4)_2$. The resulting solid solubility in $Ca_{3-x}Sr_x(PO_4)_2$, $x = 2.31$, was close to reported ones: $x \approx 2.40$ at 1000 °C[12,15] and $x \approx 2.16$ at 800 °C.[19]

All the reflections in the XRD patterns of $Ca_{3-x}Sr_x(PO_4)_2$ ($0 \le x \le 16/7$) could be indexed in a trigonal space group of *R*3*c* with lattice parameters of $a \approx 10$ Å and $c \approx 38$ Å on the basis of structural data for β-$Ca_3(PO_4)_2$.[2] Figure 1 shows portions of the XRD patterns for $Ca_{3-x}Sr_x(PO_4)_2$. Reflections with odd indices *l* in space group *R*3*c* are marked with arrows. Intensities of these reflections decreased with increasing Sr content. These reflections disappeared in solid solutions with $x \ge 13/7$. The reflections in the solid solutions with $13/7 \le x \le 16/7$ would have even indices *l* if a unit cell with $a \approx 10$ Å and $c \approx 38$ Å was adopted to index them. However, we assumed that *c* parameters in the Sr-rich phosphates are approximately equal to half the *c* parameters of the phosphates with $0 \le x \le 12/7$. With lattice parameters of $a \approx 10$ Å and $c \approx 19$ Å, reflection conditions in $Ca_{3-x}Sr_x(PO_4)_2$ ($13/7 \le x \le 16/7$) were $-h + k + l = 3n$ (obverse setting) with no extra conditions, revealing possible space groups to be *R*3, $R\bar{3}$, *R*32, *R*3*m*, and $R\bar{3}m$.

The SHG measurements at RT for samples with $x \le 9/7$ gave SHG efficiencies approximately the same as those for polar β-$Ca_3(PO_4)_2$ (Table 2). In contrast to them, samples with $13/7 \le x \le 16/7$ exhibited only negligible SHG signals. Thus, the samples with $13/7 \le x \le 16/7$ are centrosymmetric whereas those with $0 \le x \le 12/7$ are noncentrosymmetric. Rapid drops of the SHG signals in samples with $10/7 \le x \le 12/7$ are attributed to mixing of the centrosymmetric and noncentrosymmetric phases. The noncentrosymmetric modifications of $Ca_{3-x}Sr_x(PO_4)_2$ will hereinafter be referred to as β-$Ca_{3-x}Sr_x(PO_4)_2$ analogous to β-$Ca_3(PO_4)_2$ and centrosymmetric modifications as β′-$Ca_{3-x}Sr_x(PO_4)_2$. Because space groups *R*3, *R*32, and *R*3*m* are noncentrosymmetric, β′-$Ca_{3-x}Sr_x(PO_4)_2$ belongs to either space group $R\bar{3}m$ or $R\bar{3}$.

Table 2 summarizes lattice parameters of $Ca_{3-x}Sr_x(PO_4)_2$. Figure 2 shows the dependence of lattice parameters on the Sr content. No appreciable changes in the *a* and *c* parameters were detected near $x = 12/7$ where the crystal symmetry of the solid solutions changed. The resulting lattice parameters were close to the reported ones.[12,19]

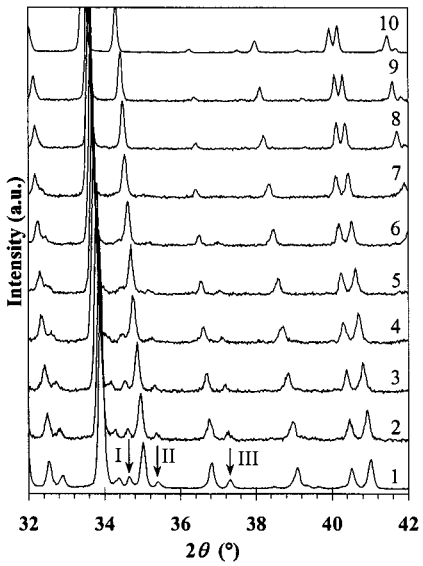

Figure 1. Portions (2θ from 32° to 42°) of XRD patterns for the solid solutions $Ca_{3-x}Sr_x(PO_4)_2$: (1) $x = 1$, (2) $x = 8/7$, (3) $x = 9/7$, (4) $x = 10/7$, (5) $x = 11/7$, (6) $x = 12/7$, (7) $x = 13/7$, (8) $x = 2$, (9) $x = 15/7$, and (10) $x = 16/7$. Arrows show the strongest reflections with odd indices *l* in space group *R*3*c* (I: 2 2 3; II: 1 3 1; and III: 3 1 5).

Table 2. Lattice Parameters, SHG Signals, and Phase-Transition Temperatures for the Solid Solutions $Ca_{3-x}Sr_x(PO_4)_2$ ($0 \le x \le 16/7$)

x	*a* (Å)	*c* (Å)	$I_{2\omega}/I_{2\omega}(SiO_2)$[a]	T_c (°C)
0	10.4300(5)	37.3815(9)	3.1	920[b]
1/7	10.4549(5)	37.4170(9)		
2/7	10.4748(5)	37.5010(9)		
3/7	10.4805(5)	37.5650(9)	3.8	780
4/7	10.5002(5)	37.6780(9)		
5/7	10.5167(5)	37.7860(9)	4.3	700
6/7	10.5375(5)	37.9160(9)		
1	10.5612(2)	38.0588(5)	1.7	675
8/7	10.5760(5)	38.1820(9)	1.2	640
9/7	10.5947(5)	38.3080(9)	0.6	610
10/7	10.6159(5)	38.4540(9)	0.18	530
11/7	10.6285(5)	38.5550(9)	0.12	530
12/7	10.6434(5)	38.6830(9)	0.04	520
13/7	10.6593(5)	19.3916(5)	0.02	
2	10.6619(5)	19.4815(5)	0.02	
15/7	10.6796(5)	19.5404(5)	0.02	
16/7	10.7015(2)	19.5787(2)	0.02	

[a] SHG signals measured after slow cooling. [b] This temperature was determined in an electrical conductivity measurement.

(42) Sugujama, K.; Tokonami, M. *Mineral. J.* **1990**, *15*, 141.

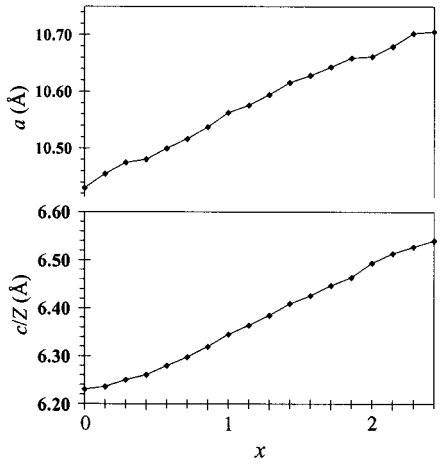

Figure 2. Lattice parameters, a and c/Z, versus Sr content, x, for the solid solutions $Ca_{3-x}Sr_x(PO_4)_2$ ($0 \le x \le 17/7$), where Z is the number of formula units per unit cell.

IR spectra of samples with $x = 0$, 1, and 16/7 (Figure 3) showed a series of absorption bands assigned to ν(P−O) and δ(O−P−O) at 1400−800 and 650−500 cm^{-1}, respectively. Some bands slightly shifted to lower wavenumbers with increasing Sr content. IR spectra for the noncentrosymmetric phases ($x = 0$ and 1) between 650 and 500 cm^{-1} (Figure 3b) were very similar to each other. On the other hand, they slightly differed from the spectrum of the centrosymmetric phase ($x = 16/7$), which may reflect a difference in crystal symmetry between the samples with $x = 0$ and 1 and $x = 16/7$. The ν(P−O) bands broadened with increasing Sr content (Figure 3a).

Phase Transitions. Figure 4 shows SHG signal versus temperature curves for the solid solutions with $0 \le x \le 12/7$. The SHG signals disappeared above some characteristic temperatures, T^+, during heating but reappeared at somewhat different temperatures, T^-, during cooling. Therefore, the $\beta \rightleftarrows \beta'$ phase transition in $Ca_{3-x}Sr_x(PO_4)_2$ ($0 \le x \le 12/7$) is reversible. This high-temperature phase transition is accompanied by transformation from a noncentrosymmetric structure to a centrosymmetric one. SHG signal values at RT decreased with increasing Sr content for $x \ge 5/7$. Table 2 summarizes transition temperatures, T_c ($T_c = T^+$), and SHG signal values, $I_{2\omega}/I_{2\omega}(SiO_2)$, for $Ca_{3-x}Sr_x(PO_4)_2$. T_c in $Ca_{3-x}Sr_x(PO_4)_2$ ($0 \le x \le 12/7$) decreased with increasing Sr content. Differences in the SHG signal values before and after the heating/cooling cycles (Figure 4) may reflect different heat treatments. As-synthesized samples were quenched from 1000 °C to RT and then heated and cooled at a rate of 5 °C/min during the SHG experiments. In other words, the differences in the SHG signal values are ascribed to nonequilibrium states of the as-synthesized samples.

Figure 5 displays the results of the DSC measurements for $Ca_2Sr(PO_4)_2$. The specific heat capacity, c_p, increased within 20−500 °C, that is, prior to the phase transition. A slight decrease in c_p was detected over the range of 500−625 °C whereas c_p decreased considerably within 625−775 °C. An increase in c_p was observed again above 775 °C.

Figure 6 shows ionic conductivity (lg σ) versus inverse temperature ($10^3/T$) curves for $Ca_3(PO_4)_2$ and $Ca_2Sr(PO_4)_2$. The curve for $Ca_2Sr(PO_4)_2$ is divided into three

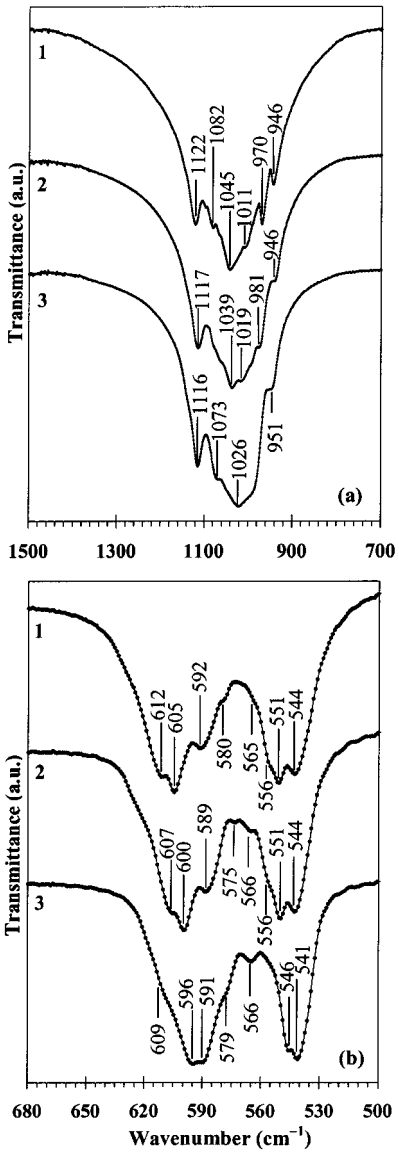

Figure 3. IR spectra in wavenumber regions of (a) 1500−700 cm^{-1} and (b) 680−500 cm^{-1} for $Ca_{3-x}Sr_x(PO_4)_2$ with Sr contents of (1) $x = 0$, (2) $x = 1$, and (3) $x = 16/7$.

temperature ranges: I (500−625 °C), II (above 775 °C) where linear changes were observed, and III (625−725 °C) where the slope of the curve monotonically decreased. The curve for $Ca_3(PO_4)_2$ is also divided into three parts: I (up to 920 °C) with a nonlinear increase, II (920−1135 °C) with a linear increase, and III (above 1135 °C) where lg σ decreased sharply.

Structure Refinements of β-$Ca_2Sr(PO_4)_2$ and β'-$Ca_{5/7}Sr_{16/7}(PO_4)_2$. The crystal structures of the samples with $13/7 \le x \le 16/7$ at RT were likely to be isotypic with the high-temperature modifications (β') of the samples with $0 \le x \le 12/7$. To clarify a structural difference between the β- and β'-modifications, the structure parameters of β-$Ca_2Sr(PO_4)_2$ and β'-$Ca_{5/7}Sr_{16/7}(PO_4)_2$ at RT were refined by the Rietveld method.

The crystal data of β-$Ca_3(PO_4)_2$[2] were used as an initial model for the Rietveld refinements of β-$Ca_2Sr(PO_4)_2$ and β'-$Ca_{5/7}Sr_{16/7}(PO_4)_2$. β-$Ca_3(PO_4)_2$ (space group $R3c$, $Z = 21$, $a = 10.439$ Å, and $c = 37.375$ Å) has six cation sites: eight-coordinated M1, M2, and M3 sites, half-occupied M4 site, distorted octahedral M5 site, and

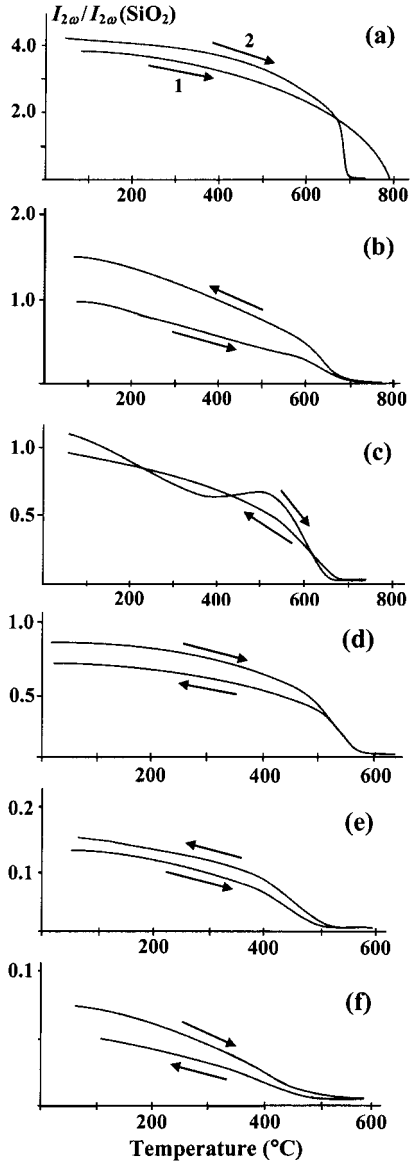

Figure 4. Dependence of the SHG signals on temperature for the solid solutions $Ca_{3-x}Sr_x(PO_4)_2$: (a) $x = 3/7$ (1) and $x = 5/7$ (2), (b) $x = 1$, (c) $x = 8/7$, (d) $x = 9/7$, (e) $x = 11/7$, and (f) $x = 12/7$. Arrows indicate heating and cooling curves.

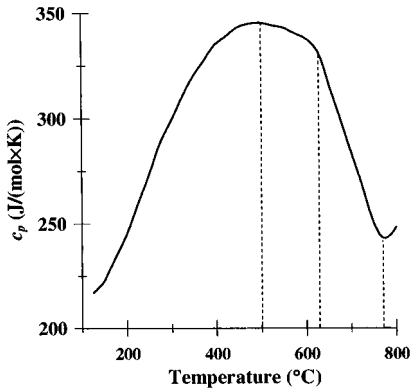

Figure 5. Specific heat capacity, c_p, versus temperature in $Ca_2Sr(PO_4)_2$.

vacant M6 site.[43] Half the M4 sites and the M6 sites are cavities surrounded by 15 and 13 O atoms, respectively.[43] The M1−M3 sites were located at general positions (18b). The M4−M6 sites were laid on the 3-fold rotation axis (6a). β-$Ca_3(PO_4)_2$ includes three phosphorus sites: P1 on the 3-fold rotation axis (6a) and P2 and P3 at general positions (18b). The M5 atom was placed at the origin (0, 0, 0) because of the arbitrariness of assigning the origin in the noncentrosymmetric space group of *R*3*c*.

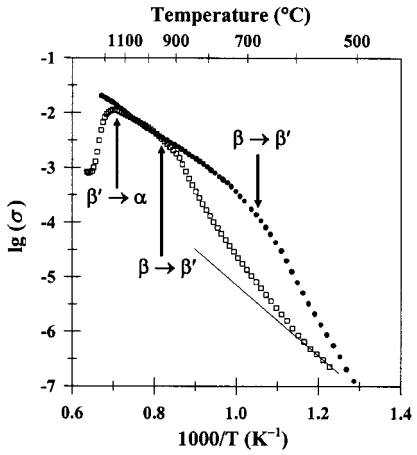

Figure 6. Plot of lg σ versus $1/T$ in $Ca_2Sr(PO_4)_2$ (black circles) and $Ca_3(PO_4)_2$ (squares). Unit of σ: S cm^{-1}.

Distribution of Ca^{2+} and Sr^{2+} ions among the M1−M5 sites was preliminarily estimated by imposing the following linear constraints on occupancies, *g*: $g(Sr) + g(Ca) = 1$ for the M1−M3 and M5 sites and $g(Sr) + g(Ca) = 0.5$ for the M4 site. The refinement of these occupancies revealed that, in both compounds, Sr^{2+} and Ca^{2+} ions are located at the M1−M4 sites whereas Ca^{2+} ions preferentially occupy the M5 site.

The subsequent Rietveld analysis of β-$Ca_2Sr(PO_4)_2$ yielded reasonable isotropic atomic displacement parameters, *B*, and interatomic distances, *l*. The composition derived from refined occupancies was close to the stoichiometric one. The M4 site proved to be occupied by Sr^{2+} ions almost exclusively. An additional linear constraint on the chemical composition (the total number of Sr^{2+} ions per unit cell is 21) and the fixed occupancy of the M4 site ($g(Sr) = 0.5$) were introduced into Rietveld refinements in the last stage. Refinement of g(M6) in β-$Ca_2Sr(PO_4)_2$ showed this site to be vacant. Therefore, we can conclude that β-$Ca_2Sr(PO_4)_2$ is isotypic with β-$Ca_3(PO_4)_2$. Table 1 lists experimental and refinement conditions, lattice parameters, *R* factors, and so forth for β-$Ca_2Sr(PO_4)_2$ together with those for β'-$Ca_{5/7}Sr_{16/7}(PO_4)_2$. Table 3 gives final fractional coordinates and *B* parameters. Figure 7a displays a portion of observed, calculated, and difference XRD patterns for β-$Ca_2Sr(PO_4)_2$.

An attempt to refine structure parameters of β'-$Ca_{5/7}Sr_{16/7}(PO_4)_2$ on the basis of the *R*3*c* model failed. The O11 site had an extraordinarily large *B* value of $\approx$40 Å^2, and most of the other *B* values for O atoms were negative. Besides, some interatomic distances, l(P−O), in all the PO_4 tetrahedra were far from reasonable: l(P−O) = (1.38−1.75) Å. Refinement of g(M6) showed that the M6 site was not vacant. These results support the idea that β'-$Ca_{5/7}Sr_{16/7}(PO_4)_2$ is structurally different from β-$Ca_2Sr(PO_4)_2$.

(43) Lazoryak, B. I. *Russ. Chem. Rev.* **1996**, *65*, 287.

Table 3. Fractional Coordinates and Isotropic Atomic Displacement Parameters for β-$Ca_2Sr(PO_4)_2$

atom[a]	site	*x*	*y*	*z*	*B* (Å^2)
M1	18b	0.7238(4)	0.8566(5)	0.4329(2)	0.76(10)
M2	18b	0.6180(4)	0.8191(6)	0.2333(2)	0.73(9)
M3	18b	0.1317(4)	0.2792(3)	0.3280(2)	1.39(8)
Sr4	6a	0	0	0.1786(3)	3.0(2)
Ca5	6a	0	0	0	0.34(11)
P1	6a	0	0	0.2650(3)	3.0(2)
P2	18b	0.6876(5)	0.8565(9)	0.1336(3)	1.51(14)
P3	18b	0.6592(7)	0.8479(7)	0.0333(3)	0.59(13)
O11	6a	0	0	0.3036(6)	1.2(5)
O12	18b	0.0184(14)	0.8713(13)	0.2551(6)	4.7(4)
O21	18b	0.7319(14)	0.9046(17)	0.1718(5)	3.6(4)
O22	18b	0.7607(16)	0.7728(14)	0.1218(4)	0.0(3)
O23	18b	0.7317(17)	0.0086(15)	0.1126(5)	0.6(3)
O24	18b	0.5221(10)	0.763(2)	0.1270(4)	0.5(2)
O31	18b	0.6069(13)	0.9472(14)	0.0476(4)	0.0(3)
O32	18b	0.5702(16)	0.6955(16)	0.0485(5)	1.8(4)
O33	18b	0.8187(10)	0.9251(15)	0.0440(4)	0.0(3)
O34	18b	0.6309(10)	0.8224(15)	0.9929(4)	0.2(2)

[a] Occupancies are g(Sr) = 0.287(8) and g(Ca) = 0.713 for M1, g(Sr) = 0.206(8) and g(Ca) = 0.794 for M2, g(Sr) = 0.506 and g(Ca) = 0.494 for M3, g(Sr) = 0.5 for Sr4, and 1 for all the other sites.

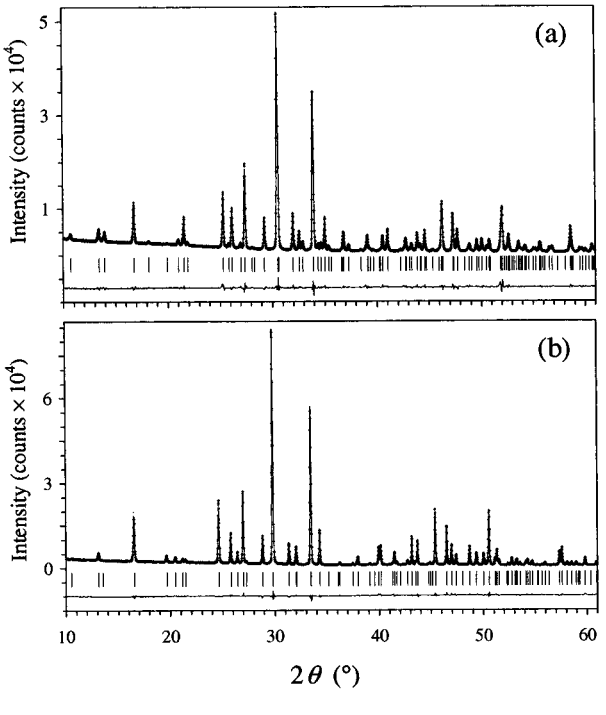

Figure 7. Portions (2θ from 10° to 61°) of observed (crosses), calculated (solid line), and difference XRD patterns for (a) β-$Ca_2Sr(PO_4)_2$ and (b) β'-$Ca_{5/7}Sr_{16/7}(PO_4)_2$. Bragg reflections are indicated by tick marks.

In subsequent Rietveld refinements of β'-$Ca_{5/7}Sr_{16/7}(PO_4)_2$, we assumed its space group to be $R\bar{3}m$ with higher symmetry than $R\bar{3}$. At first, we transformed the fractional coordinates refined with space group $R3c$ into those for space group $R\bar{3}m$. This procedure was described in more detail in the previous paper dealing with the structure refinement of $Sr_9Fe_{1.5}(PO_4)_7$[24] isotypic with β'-$Ca_{5/7}Sr_{16/7}(PO_4)_2$. In the $R\bar{3}m$ model, the M1 and M2 sites, the M4 and M6 sites, and the $P2O_4$ and $P3O_4$ tetrahedra are equivalent to each other, and the P1 (3b), M3 (9e), and M5 (3a) sites lie at centers of symmetry. For β'-$Ca_{5/7}Sr_{16/7}(PO_4)_2$, we will hereafter use the same site designations as those for β-$Ca_2Sr(PO_4)_2$.

The refinement of structure parameters of β'-$Ca_{5/7}Sr_{16/7}(PO_4)_2$ with the $R\bar{3}m$ model afforded an unreasonably large B(M3) value of 8.4(2) Å^2. Displacing M3 from the 9e site ($^1/_2$, $^1/_2$, 0) at the center of symmetry to a half-occupied 18h site (x, $-x$, z) gave B(M3) = 2.11(4) Å^2. Our single-crystal X-ray analysis of an isotypic compound, $Sr_{9.2}Co_{1.3}(PO_4)_7$, on the basis of space group $R\bar{3}m$ confirmed that M3 atoms are really disordered over four positions.[44] Further splitting of M3 atoms in β'-$Ca_{5/7}Sr_{16/7}(PO_4)_2$ into two 18h sites, M31 and M32, with g = 1/4 yielded a reasonable B parameter of 0.52(5) Å^2 with appreciably lower R factors (R_{wp} = 5.16%, R_p = 3.91%, R_B = 4.02%, R_F = 1.63%) in comparison with another refinement where one 18h site was assigned to M3 (R_{wp} = 5.94%, R_p = 4.46%, R_B = 4.55%, R_F = 2.15%).

In Rietveld refinements into which the M31 and M32 sites were introduced, the following linear constraints were imposed on occupancies: (1) g(Sr) + g(Ca) = 1 for the M1 site, (2) g(Sr) + g(Ca) = 1/4 for the M4 site, (3) g(Sr) + g(Ca) = 1/4 for the M31 site, (4) the overall occupancies of the M31 and M32 sites are equal to each other, and (5) chemical constraints on the amounts-of-substance of metals. The $P2O_4$ tetrahedron could be localized quite easily. However, we found it difficult to locate O atoms around the P1 atom; B(O11) and B(O12) were unreasonably large: B(O11) ≈ 30 Å^2 and B(O12) ≈ 10 Å^2. We explored different models for the O atoms surrounding the P1 site. The O11 and O12 atoms were respectively located at half-occupied positions 6c (0, 0, z) and 18h (x, $-x$, z) in the initial model. The best model was reached when the O11 and O12 atoms were unified to be located at a general position O11 (36i) with g = 1/3.

The $R\bar{3}m$ model gave apparently larger B parameters: B(M4) = 5.0(3) Å^2, B(P1) = 4.8(2) Å^2, and B(O11) = 9.1(5) Å^2. This finding suggests that highly disordered arrangements of these atoms cannot be represented adequately with our simple split-atom model. The application of whole-pattern fitting based on the maximum entropy method[45] to these materials would enable us to express the static disordering more satisfactorily. Very large B(M4), B(P1), and B(O11) parameters were also obtained in $Sr_9Fe_{1.5}(PO_4)_7$[24] and $Sr_{9.1}Cu_{1.4}(PO_4)_7$.[25] It should be pointed out here that β'-$Ca_{5/7}Sr_{16/7}(PO_4)_2$ must exhibit additional disordering arising from statistical distribution of Ca^{2+} and Sr^{2+} ions among the M1, M31, M32, and M4 sites.

Final fractional coordinates and B parameters for β'-$Ca_{5/7}Sr_{16/7}(PO_4)_2$ are listed in Table 4, and P−O bond lengths for β-$Ca_2Sr(PO_4)_2$ and β'-$Ca_{5/7}Sr_{16/7}(PO_4)_2$ in Table 5. Figure 7b displays a portion of observed, calculated, and difference XRD patterns for β'-$Ca_{5/7}Sr_{16/7}(PO_4)_2$.

Discussion

β-$Ca_2Sr(PO_4)_2$ is isotypic with β-$Ca_3(PO_4)_2$. In β-$Ca_2Sr(PO_4)_2$, Ca^{2+} and Sr^{2+} ions have the same tendencies to distribute among the M1−M5 sites as in another isotypic compound, $Ca_{1.5}Sr_{1.5}(VO_4)_2$.[8] That is, the M5 site is fully occupied by Ca^{2+} ions (g(Ca) = 1);

(44) Belik, A. A.; Lazoryak, B. I., unpublished results.
(45) Izumi, F.; Kumazawa, S.; Ikeda, T.; Hu, W.-Z.; Yamamoto, A.; Oikawa, K. *Mater. Sci. Forum* **2001**, *378−381*, 59.

Table 4. Fractional Coordinates and Isotropic Atomic Displacement Parameters for β'-$Ca_{5/7}Sr_{16/7}(PO_4)_2$

atom[a]	site	*x*	*y*	*z*	*B* (Å^2)
M1	18h	0.18985(4)	$=-x$	0.53595(4)	0.92(2)
M31	18h	−0.5128(2)	$=-x$	0.0071(2)	0.52(5)[b]
M32	18h	−0.5372(2)	$=-x$	0.0128(2)	0.52[b]
M4	6c	0	0	0.3504(4)	5.0(3)
Ca5	3a	0	0	0	0.84(8)
P1	3b	0	0	$^1/_2$	4.8(2)
P2	18h	0.49056(9)	$=-x$	0.39991(11)	1.30(4)
O11	36i	0.8950(14)	0.0310(16)	0.5381(4)	9.1(5)
O21	18h	0.5317(2)	$=-x$	0.6763(2)	2.73(11)
O22	36i	0.2573(3)	0.0075(3)	0.2339(2)	1.52(7)
O24	18h	0.9077(2)	$=-x$	0.0764(2)	0.61(8)

[a] Occupancies are g(Sr) = 0.838(3) and g(Ca) = 0.162 for M1, g(Sr) = 0.2200(12) and g(Ca) = 0.0300 for M31 and M32, g(Sr) = 0.165 and g(Ca) = 0.085 for M4, g(O11) is $^1/_3$, and 1 for all the other sites. [b] These parameters were constrained to be equal.

Table 5. P−O Bond Lengths (Å) in β-$Ca_2Sr(PO_4)_2$ and β'-$Ca_{5/7}Sr_{16/7}(PO_4)_2$[a]

β-$Ca_2Sr(PO_4)_2$		β'-$Ca_{5/7}Sr_{16/7}(PO_4)_2$	
P1−O11	1.47(2)	P1−O11 (×12) [b]	1.518(7)
P1−O12^{i,ii,iii} (×3)	1.514(13)	P2−O21^{v}	1.548(4)
P2−O21	1.53(2)	P2−O22^{vi,vii} (×2)	1.542(3)
P2−O22	1.504(13)	P2−O24^{viii}	1.566(3)
P2−O23	1.639(13)		
P2−O24	1.539(9)		
P3−O31	1.510(13)		
P3−O32	1.516(14)		
P3−O33	1.516(10)		
P3−O34^{iv}	1.562(13)		

[a] Symmetry codes: (i) x, $-1+y$, z; (ii) $1-y$, $1+x-y$, z; (iii) $-1-x+y$, $-x$, z; (iv) x, y, $-1+z$; (v) x, y, $1-z$; (vi) $^1/_3+x$, $^2/_3-x+y$, $^2/_3-z$; (vii) $^1/_3+x-y$, $^2/_3-y$, $^2/_3-z$; (viii) $-^1/_3+x$, $^1/_3+y$, $^1/_3+z$. [b] Bond lengths are given for all the split atoms O11.

the M4 site accommodates only Sr^{2+} ions with g(Sr) = 0.5; in the M1−M3 sites, the M3 site is mostly occupied by Sr^{2+} ions (g(Sr) = 0.506), and the M2 site is occupied by Sr^{2+} ions to the least extent (g(Sr) = 0.206).

β'-$Ca_{5/7}Sr_{16/7}(PO_4)_2$ is structurally related to β-$Ca_3(PO_4)_2$[2] and α-$Sr_3(PO_4)_2$[42] (space group $R\bar{3}m$, Z = 3, a = 5.3901 Å, and c = 19.785 Å). β'-$Ca_{5/7}Sr_{16/7}(PO_4)_2$ has a doubled a parameter in comparison with α-$Sr_3(PO_4)_2$ while β-$Ca_3(PO_4)_2$ has a doubled c parameter as compared with β'-$Ca_{5/7}Sr_{16/7}(PO_4)_2$. Figures 8 and 9 illustrate the three structures viewed along the [110] and [001] directions, respectively. α-$Sr_3(PO_4)_2$ comprises one type of layers I. Layers I contain one type of columns *B*. The structures of β'-$Ca_{5/7}Sr_{16/7}(PO_4)_2$ and β-$Ca_3(PO_4)_2$ can be constructed from the two types of layers I and II.[43] Layers I contain columns *B* whereas layers II contain columns *A* and *B*. Layers I and columns *B* are very similar to each other in the three structures.

The main differences among the three structures are seen in layers II and columns *A*. Columns *A* in β'-$Ca_{5/7}Sr_{16/7}(PO_4)_2$ differ from columns *A* ($A \infty B$) in α-$Sr_3(PO_4)_2$. That is, one PO_4 tetrahedron is orientationally disordered, and g changes from 1 (Sr2 site in α-$Sr_3(PO_4)_2$) to 0.25 (M4 site in β'-$Ca_{5/7}Sr_{16/7}(PO_4)_2$) to compensate for the removal of another PO_4 tetrahedron from columns *A* (Figure 8b,c). Columns *A* in β-$Ca_3(PO_4)_2$ are different from columns *A* in β'-$Ca_{5/7}Sr_{16/7}(PO_4)_2$ in orientational ordering of $P1O_4$ tetrahedra and metal ordering at the M4 (g = 0.5) and M6 (g = 0.0) sites (Figure 8a,b). Thus, β'-$Ca_{5/7}Sr_{16/7}(PO_4)_2$ has structural properties intermediate between β-$Ca_3(PO_4)_2$ and

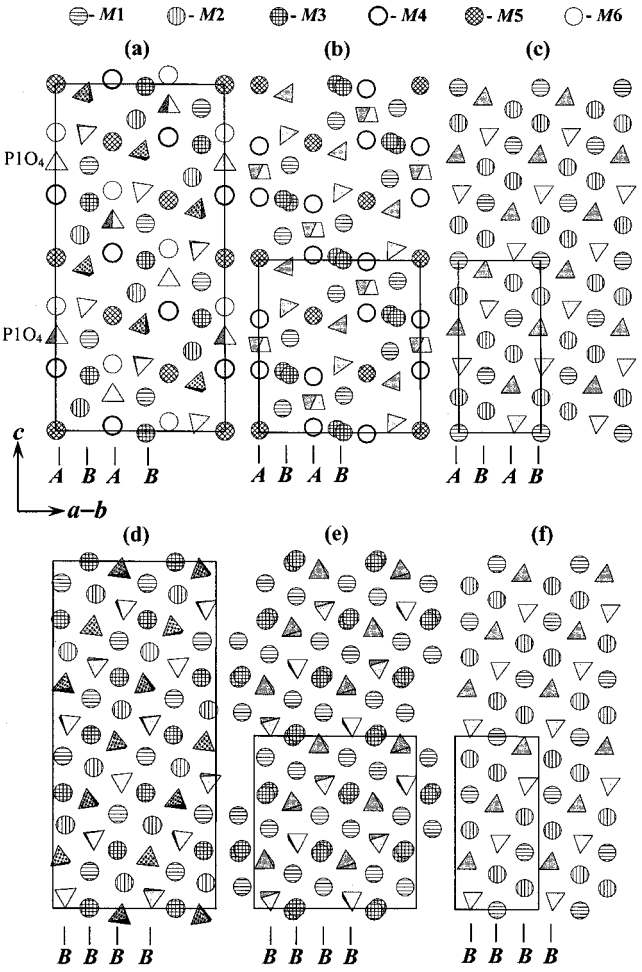

Figure 8. Layers II (a, b, c) and layers I (d, e, f) in (a, d) β-$Ca_3(PO_4)_2$, (b, e) β'-$Ca_{5/7}Sr_{16/7}(PO_4)_2$, and (c, f) α-$Sr_3(PO_4)_2$ viewed along the [110] direction. Columns *A* and *B* are marked with ticks, and unit cells of the three structures are plotted. The disordered $P1O_4$ tetrahedra and split positions M3 are shown for β'-$Ca_{5/7}Sr_{16/7}(PO_4)_2$.

α-$Sr_3(PO_4)_2$. The structure of β'-$Ca_{5/7}Sr_{16/7}(PO_4)_2$ is, however, topologically closer to that of β-$Ca_3(PO_4)_2$ because they differ only in the occupancies of the cations and orientation of phosphate ions. On the other hand, columns *A* for α-$Sr_3(PO_4)_2$ and β'-$Ca_{5/7}Sr_{16/7}(PO_4)_2$ are considerably distinct from each other.

Using the structural data for β'-$Ca_{5/7}Sr_{16/7}(PO_4)_2$ and β-$Ca_2Sr(PO_4)_2$, we will elucidate the mechanism of the high-temperature phase transition, $\beta \rightleftarrows \beta'$, in $Ca_{3-x}Sr_x(PO_4)_2$ ($0 \le x \le 12/7$). The $\beta \rightleftarrows \beta'$ phase transition is accompanied by the redistribution of cations from the M4 sites to both the M4 and M6 sites so that the occupancies of these sites are equal to each other. Because the M3 site lies between the M4 and M6 sites, the path for cation transfer is not obvious. Figure 10 illustrates a possible path of cation transfer. The disordering at the M3 sites (as found in β'-$Ca_{5/7}Sr_{16/7}(PO_4)_2$) presents evidence that cations migrate from M4 through M3 to M6. The cation disordering seems to cause orientational disordering of $P1O_4$ tetrahedra because the M3 atom is coordinated to the O11 and O12 atoms. In addition, the O11 atom cannot be situated on the 3-fold rotation axis if the M6 sites are occupied; the occupation of M6 would lead to an unreasonably short distance l(M6−O11) ≈ 0.5 Å (if z(M6) = $-z$(M4) in β-$Ca_3(PO_4)_2$).

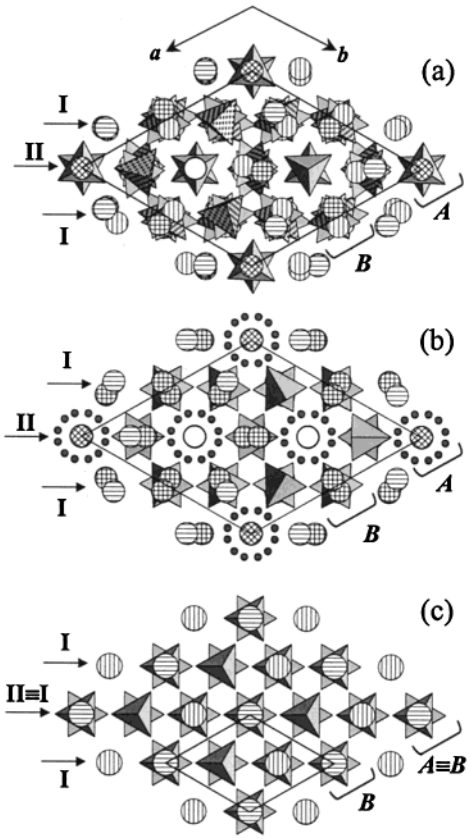

Figure 9. Crystal structures of (a) β-$Ca_3(PO_4)_2$, (b) β'-$Ca_{5/7}Sr_{16/7}(PO_4)_2$, and (c) α-$Sr_3(PO_4)_2$ viewed along the [001] direction. Layers I and II and columns *A* and *B* are respectively marked with arrows and braces, and unit cells of the three structures are plotted. The split positions O11 (small dark circles) and M3 are shown for β'-$Ca_{5/7}Sr_{16/7}(PO_4)_2$.

The $\beta \rightleftarrows \beta'$ phase transition involves the cation migration and equalization of *g*(M4) and *g*(M6). Thus, it may be classified as an order−disorder type in some temperature range as suggested for a phase transition in $Ca_3(VO_4)_2$.[46] Moreover, the existence of phases intermediate between the $R3c$ and $R\bar{3}m$ phases was put forward for $Ca_3(VO_4)_2$.[46] Note that no solid solutions $Ca_{3-x}Sr_x(PO_4)_2$ ($0 \le x \le 12/7$) with the β'-type structure could be obtained at RT even by quenching to liquid N_2.

In the samples with small *x* values, the SHG signal disappeared rather abruptly with increasing temperature (Figure 4a). The $I_{2\omega}(T)$ curves smoothed in the phase transition region with increasing Sr content (Figure 4b−e), and a very weak SHG response ($I_{2\omega}/I_{2\omega}$ (SiO_2) < 0.1) was detected in the sample with $x = 12/7$ (Figure 4f) prior to the phase transition.

We can advance two possible reasons for the propagation of the phase transition in $Ca_{3-x}Sr_x(PO_4)_2$. The first reason is the nonuniform distribution of chemical species over some isolated nano- or microregions. This phenomenon is generally the main driving force of the propagation of phase transitions in the so-called relaxor-type ferroelectrics of complex chemical compositions.[47]

The second reason is derived from the Gibbs rule for phase equilibria in multicomponent systems. In the case of two-component systems with one variable quantity

(46) Grzechnik, A. *Chem. Mater.* **1998**, *10*, 1034.
(47) Lines, M. E.; Glass, A. M. *Principles and Application of Ferroelectric and Related Materials*; Clarendon Press: Oxford, 1977.

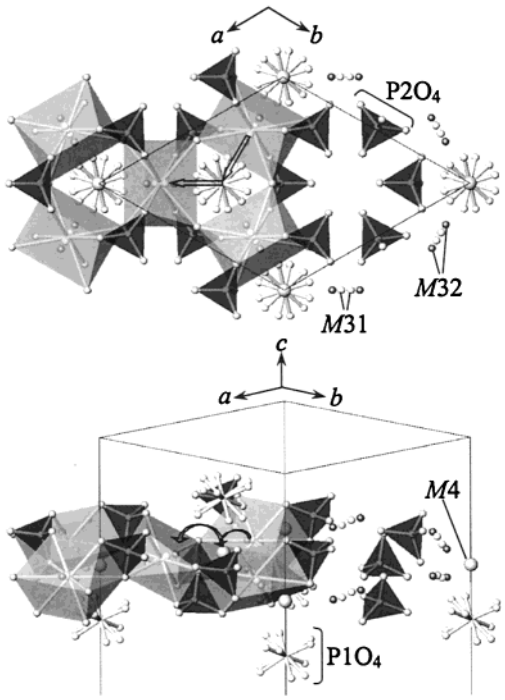

Figure 10. Relationship between the M4 and M31 (M32) sites in β'-$Ca_{5/7}Sr_{16/7}(PO_4)_2$. Polyhedra for the ideal M3 sites (9e) and $P2O_4$ tetrahedra are emphasized. Arrows show the path of cation migration, M3 → M4 → M3.

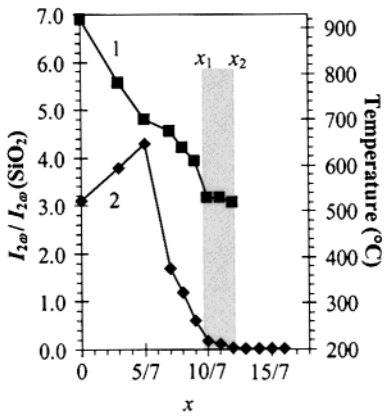

Figure 11. Temperatures, T_c (1), of the $\beta \rightleftarrows \beta'$ phase transitions and the SHG signal values, $I_{2\omega}/I_{2\omega}$ (SiO_2) (2), at RT plotted against the Sr content, *x*, for the solid solutions $Ca_{3-x}Sr_x(PO_4)_2$. The two-phase region, $x_1 \le x \le x_2$, is marked with a shaded rectangle.

(*x* in the present case), this rule predicts the existence of an intermediate two-phase region separating single-phase regions in the *T*-diagram. This two-phase region has macroscopic character.

The boundaries of the two-phase region (at RT) for the as-synthesized samples can be estimated from the SHG and XRD data. Figure 11 displays the dependence of the SHG signal and phase-transition temperature on the Sr content. The SHG signals and reflections with odd indices *l* both disappeared in the solid solutions with $x \ge 13/7$. Hence, one boundary of the two-phase region, x_2, can be assigned to that corresponding to $x_2 = 13/7$. Another boundary of the two-phase region, x_1, can hardly be determined by XRD because the XRD patterns may contain reflections of the β- and β'-phases in compounds with $x_1 \le x \le x_2$. However, x_1 can be

estimated from the SHG data. Figure 11 shows that the SHG values and T_c's are virtually constant for compositions with $10/7 \leq x \leq 12/7$, which suggests that this x region corresponds to the two-phase region. Accordingly, an x_1 value of 10/7 can be assigned to another boundary of the two-phase region.

The temperature range where a mixture of the β- and β'-phases is stable may vary from zero at $x = 0$ to a particular value on the solid-solution boundary. No boundary of the two-phase region can be determined as a function of temperature only with the available data. The temperature of the phase transition determined by the SHG method (Table 2 and Figure 11) is believed to correspond to an average value, which is confirmed by the DSC data. The specific heat capacities, $c_p(T)$, can be used to understand the mechanism of the phase transition from a thermodynamic point of view. The $c_p(T)$ value for $Ca_2Sr(PO_4)_2$ stopped to increase just before the structural transformation to the β'-phase (Figure 5) whereas it sharply decreased above 625 °C. The temperature range of 625−775 °C corresponds to the $\beta \rightarrow \beta'$ phase transition. The $c_p(T)$ value in this range reflects contributions of the β- and β'-phases. A slight decrease in $c_p(T)$ between 500 and 625 °C is probably caused by fragments of the high-temperature β'-phase formed in the bulk of the low-temperature β-$Ca_2Sr(PO_4)_2$ phase. The $c_p(T)$ curve had the minimum at 775 °C corresponding to the temperature of termination of the phase transition. According to the SHG data for $Ca_2Sr(PO_4)_2$ (Figure 4b), T_c is equal to 675 °C, which lies inside the temperature range of 625−775 °C where the two phases coexist. Contents of the polar and centrosymmetric phases are most probably comparable at 675 °C.

The dependence of the electrical conductivity on temperature in $Ca_2Sr(PO_4)_2$ correlated with the SHG and c_p data (Figures 4−6). Within the temperature range (below 775 °C) where the β-phase is stable, the electrical conductivity, lg σ, noticeably increased with increasing temperature. Apparent activation energies at 500−625 °C were close to 2.6 eV, which is too high to be associated with the migration energy of Ca^{2+} ions in $Ca_2Sr(PO_4)_2$. Such a conductivity change may be caused by the structural phase transition between 500 and 775 °C. The reconstructive transformation strongly enhances the probability that Ca^{2+} ions jump from one position to another. Such migration behavior is usually caused by changes in the concentration of charge carriers or those in the number of sites available for cation migration in the structure. After the finish of the $\beta \rightarrow \beta'$ phase transition in $Ca_2Sr(PO_4)$ at 775 °C, the lg σ versus $1/T$ curve became almost linear (Figure 6) with an activation energy of ≈1 eV. In the temperature range of 625−775 °C where the two phases coexist, the slope of the lg σ versus $1/T$ curve gradually decreased (Figure 6).

In $Ca_3(PO_4)_2$, a noticeable increase in lg σ was observed up to ca. 920 °C. Between 920 °C and 1135 °C, the lg σ versus $1/T$ curve was linear with an activation energy of about 1 eV. A sharp decrease in the conductivity above 1135 °C results from the transition of
$Ca_3(PO_4)_2$ into its α modification[28] structurally similar to β-$K_2(SO_4)_2$.[48] Conductivities and activation energies for $Ca_3(PO_4)_2$ and $Ca_2Sr(PO_4)_2$ were almost the same over the range of 920−1135 °C. This finding shows that, in this temperature range, they are isotypic with each other, with the same manner of Ca migration.

The data described above suggest that $Ca_3(PO_4)_2$ is transformed into the α-phase through a new β'-phase. The phase transition from β-$Ca_3(PO_4)_2$ to β'-$Ca_3(PO_4)_2$ is of a "polar-to-centrosymmetric" type. In contrast to the $\beta \rightarrow \beta'$ transition, the $\beta' \rightarrow \alpha$ transition in $Ca_3(PO_4)_2$ is accompanied by significant reconstruction of the whitlockite-related structure into the β-K_2SO_4-type one.[48] The $R3c \rightleftarrows R\bar{3}m$ phase transition was detected at 1110 °C in $Ca_3(VO_4)_2$[46,49] isotypic with β-$Ca_3(PO_4)_2$.[50] We have recently found similar phase transitions in two whitlockite-like compounds, $Ca_{1.5}Sr_{1.5}(VO_4)_2$[8] and $Ca_9M(PO_4)_7$ (M = Fe and In).[51,52]

The substitution of Sr for Ca in $Ca_3(PO_4)_2$ lowers the temperature of the $\beta \rightarrow \beta'$ phase transition but raises that of the $\beta' \rightarrow \alpha$ phase transition.[12,15] The temperatures of the $\beta \rightarrow \beta'$ phase transition dropped in solid solutions $Ca_{3-x}Nd_{2x/3}(VO_4)_2$.[53] This finding is explained in terms of the acceleration of the $\beta \rightarrow \beta'$ phase transition by introducing additional vacancies into the M4 site in heterovalent substitution $3Ca^{2+} \rightarrow 2Nd^{3+} + \square$. Formation of additional vacancies decreases the amount of cations that would migrate and facilitate the rotation of $V1O_4$ tetrahedra. In $Ca_{3-x}Sr_x(PO_4)_2$, g(M4) hardly changed, but their structures are relaxed by substituting Sr^{2+} ions in 8-fold coordination (effective ionic radius[54] $r = 1.26$ Å) for Ca^{2+} ions ($r = 1.12$ Å). This substitution will increase atomic mobility in the whitlockite-like structure.

Acknowledgment. This work was partially supported by the Russian Foundation for Basic Research (Grants 00-03-32660, 01-03-06122, and 01-03-06123). A.A.B. acknowledges the award of the STA Fellowship from the Japan Science and Technology Corporation.

CM020243L

(48) Robinson, M. T. *J. Phys. Chem.* **1958,** *62*, 925.
(49) Glass, A. M.; Abrahams, S. C.; Ballman, A. A.; Loiacono, G. *Ferroelectrics* **1978**, *17*, 579.
(50) Gopal, R.; Calvo, C. *Z. Kristallogr.* **1973**, *137*, 67.
(51) Lazoryak, B. I.; Morozov, V. A.; Belik, A. A.; Stefanovich, S. Yu.; Grebenev, V. V.; Leonidov, I. A.; Mitberg, E. B.; Davydov, S. A.; Lebedev, O. I.; Van Tendeloo, G., submitted to *Chem. Mater.*
(52) Morozov, V. A.; Belik, A. A.; Stefanovich, S. Yu.; Grebenev, V. V.; Lebedev, O. I.; Van Tendeloo, G.; Lazoryak, B. I. *J. Solid State Chem.* **2002**, *165*, 278.
(53) Leonidov, I. A.; Leonidova, O. N.; Surat, L. L.; Kristallov, L. V.; Perelyaeva, L. A.; Samigulina, R. F. *Russ. J. Inorg. Chem.* **2001**, *46*, 268.
(54) Shannon, R. D. *Acta Crystallogr.* **1976**, *A32*, 751.